BROADBAND SEISMIC STUDIES IN SOUTHERN ASIA: SOURCE AND PATH CHARACTERIZATION

Keith Priestley,[1] Alessia Maggi,[1] Vinod K. Gaur,[2] Supriyo Mitra,[1] Jessie L. Bonner,[3] and James F. Lewkowicz[3]

Cambridge University,[1]
Center for Mathematical Modeling and Computational Sciences, Bangalore, India,[2] and
Weston Geophysical Corporation[3]

Sponsored by Defense Threat Reduction Agency

Contract No. DTRA01-00-C-0028

ABSTRACT

We have deployed a sparse network of nine broadband stations in India to collect seismic data for studies of the crust and upper mantle velocity and attenuation structure, regional wave propagation characteristics, seismic sources, and seismic hazards. To date, our primary focus has been the installation and operation of the seismic stations, the determination of crustal structure of the southern Indian shield, and waveform modeling of earthquake sequences.

Travel times between sources and stations in the Indian shield are used to develop *P*- and *S*-wave velocity models for the Indian peninsula. Arrival times are measured in the distance range 200 to 2400 km. We minimize travel-time errors by only using sources whose hypocentral parameters are constrained with local seismic data. At near-regional distances the *Pn* and *Sn* velocities are 8.10 km/sec and 4.70 km/sec, which agree with previous results from receiver function studies. These new and/or updated velocity models have been integrated into WINPAK3D (Reiter *et al*., 2001) and are currently being validated using various sources of ground truth data in the region.

We have modeled teleseismic and regional waveforms of the 26 January 2001 Bhuj mainshock and its aftershocks. The propagation paths to the regional seismographs were calibrated by using the source mechanism and depth determined by inverting the teleseismic P- and SH- body waves of the large aftershock that occurred on 28 January 2001 and inverting the regional waveforms for the propagation characteristics of the path. We then use the regional waveforms and the calibration information for the regional paths to determine mechanisms and depths for the smaller aftershocks. We use an adaptive forward modeling approach, which efficiently samples the entire space of focal parameters and converges to the minimum misfit solution. This approach is similar to the neighborhood algorithm of Sambridge (1999). The variation in aftershock location and mechanisms suggests that more than one fault was active during the Bhuj earthquake sequence.

OBJECTIVES

The objectives of our research effort are fourfold. The first is to increase the amount of high quality seismic data that are available by deploying additional seismic stations in the India/Pakistan region. The second is to use these data to refine the regional attenuation characteristics, the regional travel time corrections, and the crust and upper mantle structure of the region. The third is to use the analysis of these data to refine Weston's 3D velocity model for India and Pakistan (WINPAK3D) and to validate the model. The fourth is to provide a cooperative forum for the exchange of information and ideas on the analysis of the data and modeling of the region.

RESEARCH ACCOMPLISHED

Operation of Broadband Seismographs in India

We currently have nine broadband seismic stations collecting seismic data in India as shown in Figure 1. This includes three new stations (BOMD, ALMO, and NAPG) together with six stations that have been in operation intermittently since early 2001. These stations are operated by Cambridge University in conjunction with the Indian Institute of Astrophysics (IIA) at Bangalore. Each station consists of a Guralp CMG-3T digital output seismometer with a velocity response between 0.008 and 50 Hz. The stations continuously sample data at 100 samples/sec, and the data are archived on 9 GB disks. Several of the stations suffered mechanical and power failures during the past year, resulting in modifications to the systems. As a result, dial-up capabilities were developed and will be installed at most of the stations by September 2002 in order to give the operators easy access to troubleshooting the systems. As we enter the final year of this project, the entire network has been deployed and is in operation.

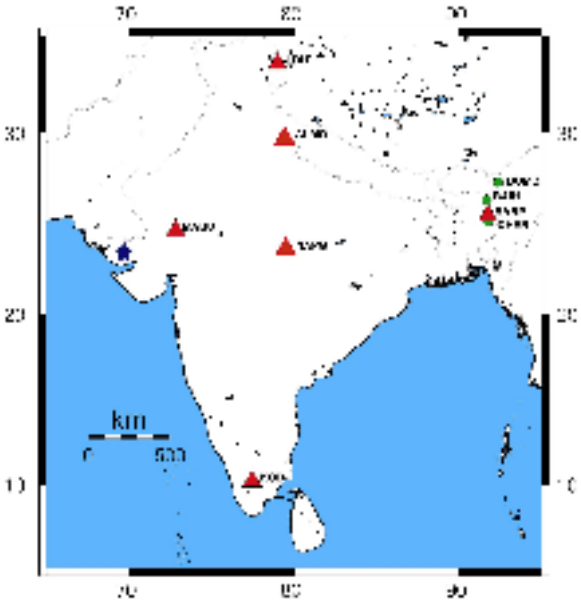

Figure 1. (Left) Locations of the Cambridge University/IIA broadband seismic stations. The stations marked with red triangles will remain deployed for the duration of the experiment while the green circles show stations that will be redeployed for optimal data coverage.

Updating the WINPAK3D Velocity Model

We continue to use the products derived from these new data collected in southern Asia to update Weston Geophysical Corporation's INdia and PAKistan 3D velocity model, referenced as WINPAK3D. The initial 3D velocity model was developed through synthesis of pertinent data from approximately 69 published references on the velocity structure, geology, and tectonics throughout the region. The references utilized included data such as seismic refraction and reflection studies, interpretations of gravity data, surface wave studies, and receiver function analyses. Stable shield regions make up a significant portion of the model to the SE, while continental collision has complicated much of the structure in the north. Recently, the model was updated using a fully 3-D tomographic inversion as described in Reiter *et al*., (2001).

Station MABU is located in northwestern India (Figure 1) approximately 300 km northwest of the Mw=7.6 Bhuj earthquake that occurred on 26 January 2001 (blue star in Figure 1). The station was deployed after the mainshock on 18 March 2001 and immediately started recording aftershocks from this region including a M_s=4.9 that occurred on 19 March 2001 (Figure 2). During the initial three weeks of MABU operation, we noted over 700 detections associated with aftershocks from this region. Figure 2 shows an example of further WINPAK3D development using these new data. We then used WINPAK3D as the starting model and inverted the Rayleigh dispersion curves for shear wave velocity structure. The results show the crustal thickness in this region is approximately 40 km and there are differences between the inverted model and WINPAK3D in the upper and middle crust. We continue to examine the events in this region for further constraints on velocity structure in northwestern India.

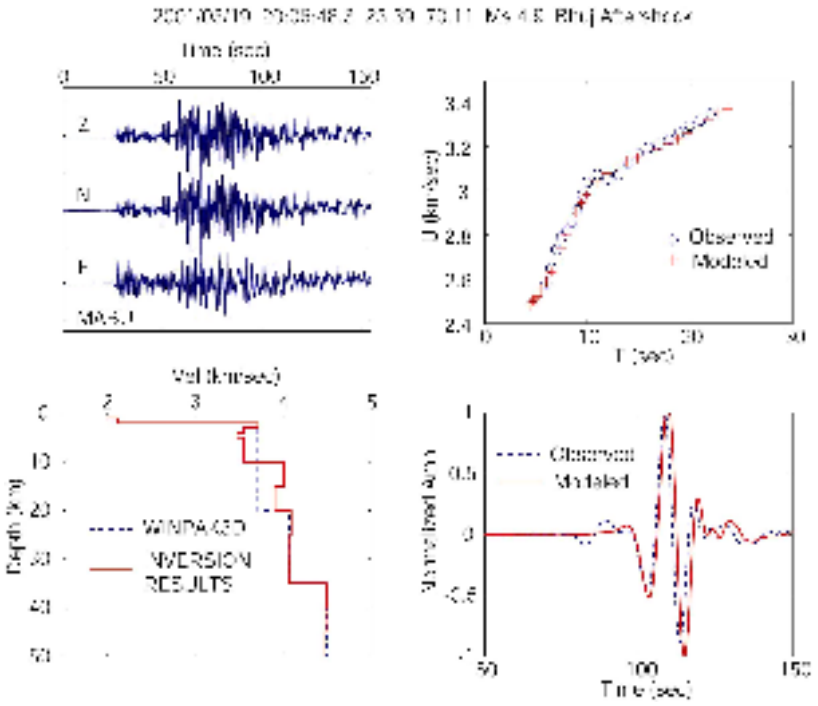

Figure 2. (Upper Left) Three-component seismograms at MABU for a Bhuj earthquake. (Upper Right) Observed and modeled dispersion curves for the Rayleigh waves from this aftershock. (Lower Left) Initial (WINPAK3D) and final model from the inversion of the Rayleigh wave dispersion curves. (Lower Right) Comparison of observed and modeled surface waves using the final model from the inversions.

<u>Source Mechanisms of Bhuj Aftershocks from Regional Waveform Modeling</u>

The Mw 7.6 earthquake of 26 January 2001 occurred in the Kachcch Peninsula (Figure 3), an area with a long history of strong earthquakes (Bapat *et al*., 1983). The region is bordered to the north and south by rift systems, created during the initial separation of the Indian subcontinent from Pangea. These structures are now subjected to compressional stress and reverse faulting resulting from the India - Eurasian collision (Talwani and Gangopadhyay, 2001). The 1819 Allah Bund earthquake, which occurred on a fault bounding the northern side of the Great Rann, was the first large earthquake in this region for which some focal mechanism information is available (Bilham, 1998). There have been other significant earthquakes in this region, the best located being the 1956 event near the town of Anjar (Figure 3).

In the following study, we examine source mechanisms for the mainshock and larger aftershocks of the Bhuj earthquake sequence. We invert teleseismic P- and SH-waveforms to determine the mainshock mechanism. We determine the mechanisms of the moderate size aftershocks from inversion of regional waveforms after calibrating the propagation paths.

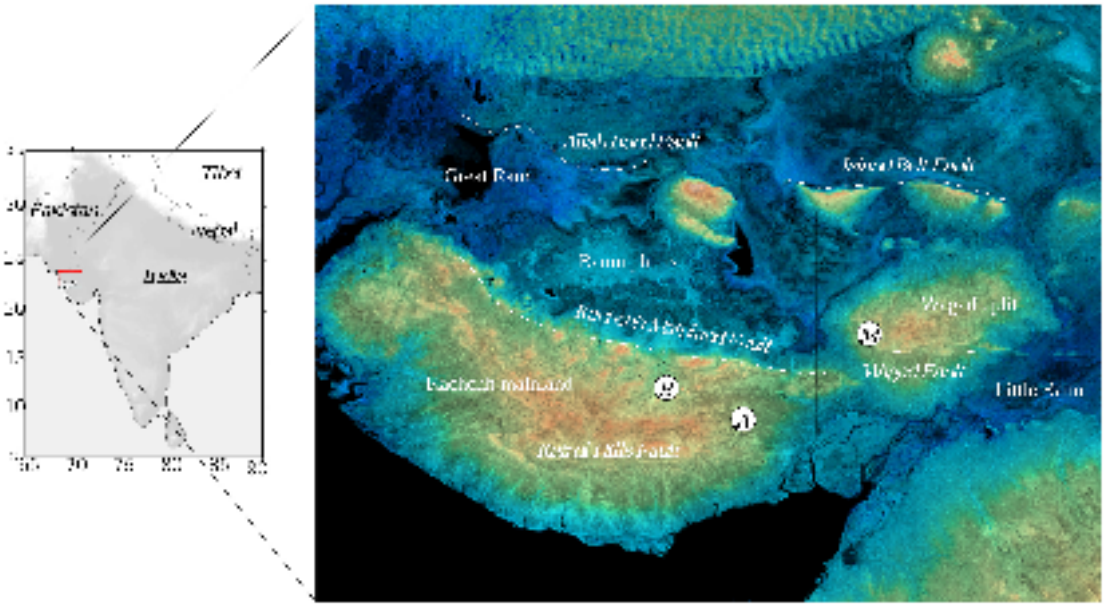

Figure 3. (Left) Geographical location of the Kachchh region and topography (right) from the Shuttle Radar Topography Mission (NASA/JPL/NIMA). Superimposed on the topography image are the locations of the major faults and the towns mentioned in this paper (B: Bhuj, A: Anjar, M: Manfara).

Teleseismic waveform modeling

The focal mechanism and depth of moderate-sized earthquakes can be determined through teleseismic body wave modeling. We invert P- and SH-waveform data for strike, dip, rake, centroid depth, seismic moment and source time function for the Bhuj mainshock and the largest aftershock (28 January). Another aftershock, 19 February, was well recorded at a few teleseismic stations and we used these data to confirm our regional solution for this event.

The Bhuj mainshock waveforms are fit by a single double couple source (Figure 4a). The minimum misfit solution is an EW trending thrust (strike 281°, dip 42°, rake 107°), with a centroid depth of ~20km. The centroid depth is constrained by the width of the larger pulses in both the P- and SH-waveforms, while the strike of the fault plane is primarily constrained by the polarity and amplitude of the SH arrivals. Our solution is consistent with the Harvard CMT solution (strike 298°, dip 39°, slip 136°). Fault-slip distribution studies (Yagi and Kikuchi, 2001; Antolik and Dreger, 2001) found that most of the slip occurred at depths of 18-25 km, with almost no slip occurring at the surface, consistent with the lack of a substantial surface faulting (Wesnousky *et al*., 2001). The rupture nucleated in the bottom half of the fault plane, and propagated westwards about 40 km and upwards about 20 km.

The 28 January event was the largest aftershock of the Bhuj earthquake, and occurred at the northern edge of the Wagad Uplift (Figure 3). The teleseismic waveforms for this earthquake (Figure 4b) are similar to those for the mainshock, except for the narrower width of the first pulse, which is controlled by both the depth and duration of the event. The body wave inversion (Figure 4b) solution for this event gives an E-W trending thrust fault (strike 81°, dip 50°, rake 87°) with a centroid depth of ~9 km and a 4 second duration. The strike of the solution is controlled by the SH waves, but is less well constrained than that of the mainshock, because the seismograms are noisier.

Regional waveform modeling

Method: The remaining large aftershocks did not produce sufficient good quality teleseismic body-waveforms to determine their source parameters from body wave modeling, and we have instead constrained their source parameters by regional waveform modeling. The character of a seismic waveform is determined by both the seismic structure along the propagation path and the earthquake source. It is more difficult to determine source properties from regional data because of the greater propagation path complexity, but source parameters can be determined from regional seismic data if the contribution from the propagation path is known. We calibrate the propagation paths to the regional stations (Figure 5) using the seismograms of the 28 January event, and then using these calibrated propagation characteristics, extract focal parameter information from the regional seismograms of the

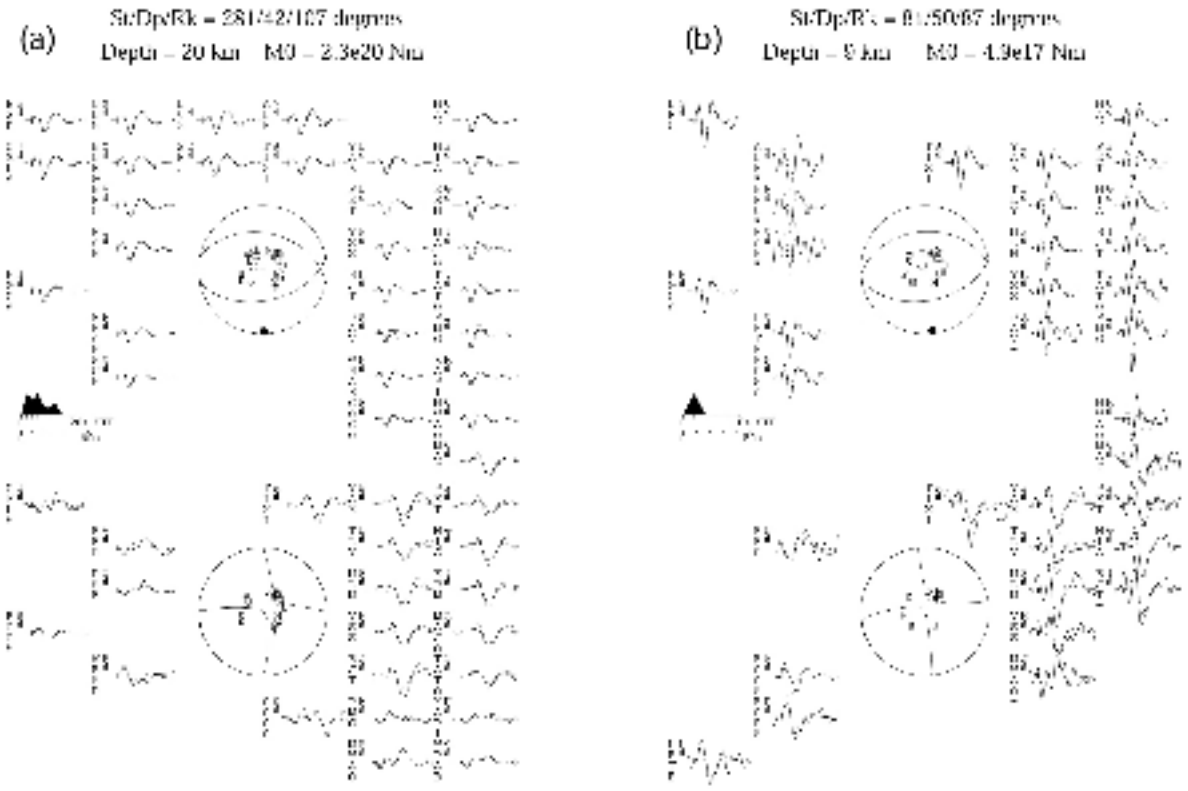

Figure 4. (a) Minimum misfit solution for the Bhuj mainshock. The upper sphere shows the P-wave radiation pattern and the lower sphere the SH-wave radiation patter. Both are lower hemisphere projections. The station code by each waveform is accompanied by a letter corresponding to its position in the focal sphere. The positions are ordered clockwise by azimuth. The solid lines are the observed waveforms, the dashed lines are the synthetic waveforms. The inversion window is marked by solid bars at either end of the waveform. P and T axes within the sphere are represented by solid and open circles, respectively. The source time function is shown below the P focal sphere, with the waveform time scale below it. (b) Minimum misfit solution for Mw 5.7 aftershock of 28 January is shown in the same format as (a).

smaller events. We calibrate the propagation paths using the 28 January aftershock rather than the mainshock because of the extended rupture of the mainshock and because the recordings at several of the closer stations were clipped.

We use a surface-waveform fitting algorithm (Nolet, 1990), which applies perturbations to depth-parameterized 1D starting models to fit multimode surface waves in increasingly wide frequency bands. We create starting models for each path by integrating along Crust2 (Bassin *et al*, 2000) and adding this to the upper mantle structure of PREM, and have parameterized both shear wave velocity ( ) and Moho depth. We have calibrated Rayleigh and Love waves separately since we require the propagation characteristics and not the velocity model. The locations of the stations and an example of path calibration are shown in Figure 5. Only three of these stations are part of the Global Seismograph Network (GSN); other data are from proprietary data sources.

Adaptive grid search: Having calibrated the propagation characteristics of paths to regional stations, we then extract focal mechanism information from surface wave recordings of the aftershocks at these stations. We use an adaptive forward modeling approach, which efficiently samples the entire space of focal parameters (strike, dip, rake, depth). This approach is similar to the neighborhood algorithm of Sambridge (1999) and is summarized in Figure 6.

Figure 5. (a) Location of broadband stations within regional distances of Bhuj. GSN stations are shown as squares, while other data sources are shown as stars, circles, and triangles. The station at Bhuj is also plotted for reference. (b) Love wave calibration of the path to central India, showing the initial and final fit of synthetic (dotted lines) seismograms and spectra to the data (solid lines). The right hand panel contains the starting (solid) and final (dotted) Earth models.

We take a random sample of points in parameter space, calculate forward synthetic seismograms by modal summation for all stations that recorded the event using the calibrated structure for each path, and compare the synthetic seismograms to the observed records to give a single misfit value per point in parameter space. We then subdivide the entire parameter space into subspaces around each sample point, such that each point within a subspace is closer to the sample point at its center than any other sample point (subdivision into Voronoi cells). 'Closeness' is defined by a Euclidean distance metric which is normalized by the a priori variances of the single parameters. We rank the sample points according to misfit, and take new random samples within the Voronoi cells around the best few sample points (best 10%). By iterating this procedure, it is possible to quickly and efficiently converge to the minimum misfit region of parameter space, mapping out deep local minima, but not getting trapped in them.

We measure the misfit, *e*, between an observed record and its synthetic seismogram by cross-correlation (Wallace, 1986):

$$e = 1 - \frac{s \quad d}{(s \quad d)^{\frac{1}{2}} (d \quad d)^{\frac{1}{2}}}, \qquad (1)$$

where *s* is the synthetic seismogram, *d* is the observed seismogram and indicates 'the maximum value of the correlation function'. Comparing seismograms in this manner allows us to cope with errors in the epicentral locations of the events. Errors in epicentral location cause the synthetic seismograms to be shifted in time with respect to the observed seismograms. These time shifts translate directly into the lag of the cross-correlation function, but do not affect its amplitude or the misfit *e*.

Results: We use this method outlined to extract focal parameter information for six of the larger aftershocks of the Bhuj earthquake. The resulting focal mechanisms and depths are listed in Table 1 and examples of the analyses are shown in Figures 7 and 8. As a test of the method, we first analyzed the 28 January aftershock. The mechanism determined from the regional seismic data for this event (Figure 7a) agrees very well with the teleseismic solution (Figure 4b) for both focal mechanism and depth. Both depth and dip have wide minima; the minimum misfit region spans depths from 5 to 12 km, and dips from 25° to 60°. There is an indication of trade-off between strike and rake, although the minimum is narrow in both these parameters. The fits to the 10 Rayleigh and 7 Love waves observed for this event at regional stations are excellent.

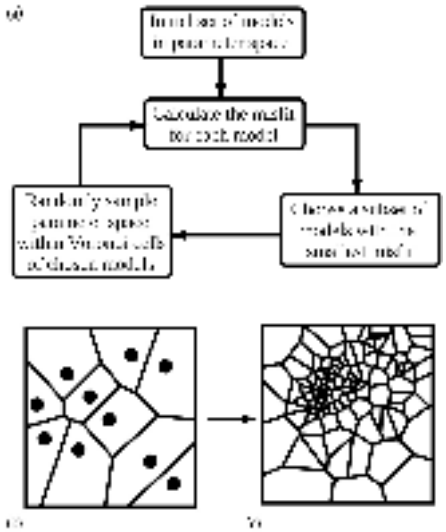

Figure 6. The neighborhood algorithm. (a) Flowchart of the adaptive grid-searching method. (b) Example of an initial distribution of parameters within a parameter space. (c) Example of a final distribution of parameters within a parameter space. (b) and (c) are reproduced from Sambridge (1999).

Table 1. Locations and focal mechanisms of the Bhuj mainshock and larger aftershocks.

DATE	TIME	LAT. N	LON. E	M_W	DEPTH	FOCAL MECHANISM
26-01-2001	03:16:40	23.415	70.322	7.5	20	281/42/107
27-01-2001	04:36:06	23.404	70.107	5.2	13	104/39/105
28-01-2001	01:02:12	23.541	70.587	5.7	9	096/48/107
03-02-2001	03:04:35	23.712	70.525	5.1	1	127/33/056
08-02-2001	16:54:42	23.705	70.475	5.2	5	141/65/167
19-02-2001	08:24:21	23.596	70.158	5.2	4	004/28/136
04:03:2001	07:54:22	23.134	70.493	5.0	11	036/86/332

Epicenters from Engdahl and Bergman (2001) except aftershock on 27-01-2001 (proprietary data). Depths and mechanisms from regional waveform inversion except the mainshock (- teleseismic waveform inversion).

Although the 27 January, 2001 (Mw 5.2) event was well recorded at six regional stations, the minimum misfit solution shows good fits to both Love and Rayleigh waveforms (Figure 7b) at stations AAK, ABKT, LSA, and (though to lower frequency) TPT. The fits at stations GBA and PUNE are less convincing. Although the minimum misfit region is small, the 10% acceptability contour encompasses a wide range of depths (0-15 km) and dips (20-70). The minimum misfit focal mechanism, an E-W trending thrust, is similar to both the mainshock and the January 28 aftershock.

The mechanism for the 19 February, 2001 (Mw 5.2) event determined from the regional seismograms is shown in Figure 8. Fits to all seismograms are good, although the synthetic seismograms do not fit the long period start of the Love wave at ABKT or the tail of the Rayleigh wave at ASH very well. This event was large enough to have a Harvard CMT solution: an E-W trending thrust mechanism also at a depth of 4 km, significantly different from the mechanism shown in Figure 8a (a NW-SE trending thrust). Figure 8b-c compare our solution with the Harvard CMT solution. Synthetic seismograms for the Harvard mechanism (Figure 8b) produces poorer fits at all stations, except for the Love wave at ABKT. This event was also large enough to produce several teleseismic P- and SH-waveforms which could be modeled. Figure 8c compares fits for four P and two SH waveforms for our mechanism and the Harvard CMT mechanism. Both solutions fit the seismograms reasonably well, with our mechanism giving a synthetic waveform fitting significantly better only at LBTB.

CONCLUSIONS AND RECOMMENDATIONS

The regional waveform grid-search analysis of the larger aftershocks of the Bhuj earthquake finds that the depths of the events are poorly constrained by the surface wave data. After depth, fault dip is the least well-constrained parameter, while fault strike and slip (rake) direction can be very well constrained by the surface wave data. Only

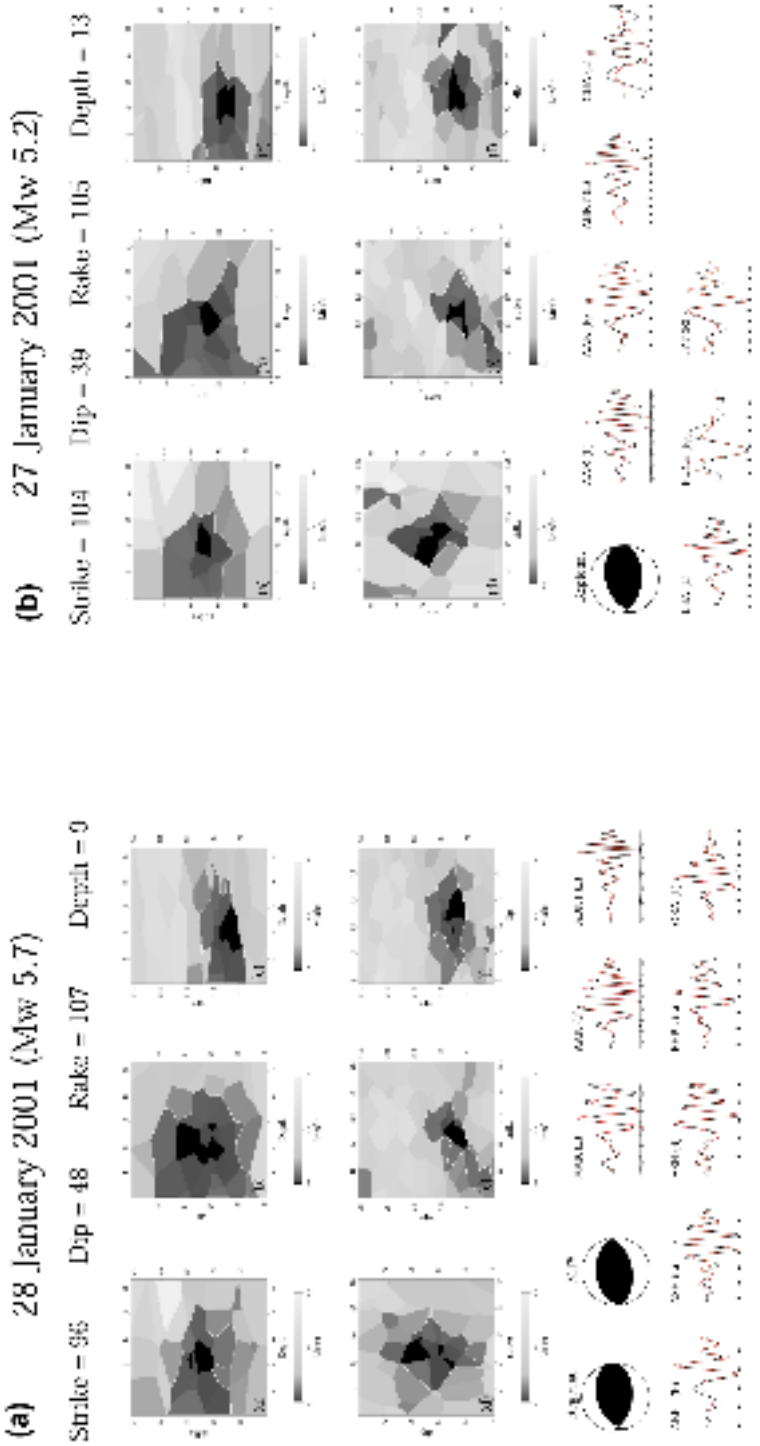

Figure 7. (a) Regional waveform solution for the 28 January aftershock. The focal parameters for the minimum misfit solution are shown under the event date. The six upper panels show slices through the misfit volume taken through the minimum, with two different parameters fixed at the minimum misfit values. Regions with misfits of less than 1% are shown in black, and regions with misfits of less than 10% are surrounded by a white contour. The regional and teleseismic mechanisms are shown below the panels, and are followed by the fits of synthetic (red dotted) to observed (solid) seismograms for all the available data. The letters (L) and (R) after the station names indicate the seismograms are Love and Rayleigh waves respectively. All parameters are very well constrained, and the resulting focal mechanism is almost identical to the teleseismic solution. (b) Regional waveform solution for the 27 January aftershock in the same format as (a). All parameters are well constrained, despite the low number of waveforms available (7), but the dip and depth have broad 10% contours. The minimum misfit focal mechanism is almost identical to the mainshock.

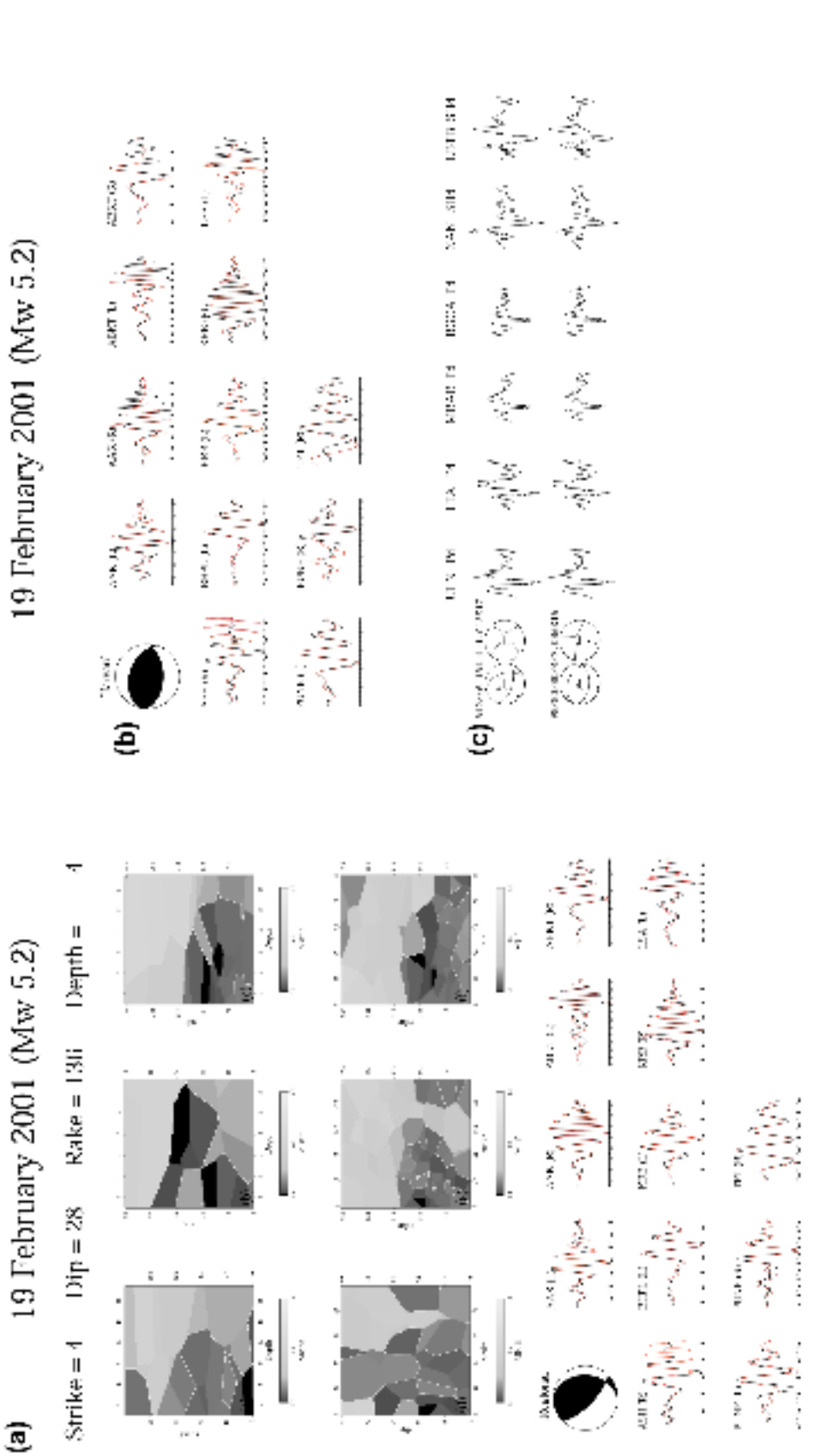

Figure 8. Regional waveform solution for the 19 February aftershock. Comparison with the Harvard CMT solution for the 19 February aftershock. (b) Fits to the regional data: the seismograms are less well matched at all stations, except for ABKT, where the long period precursor to the Love waves is better matched by the CMT solution. (c) Fits to the teleseismic data. The first line shows the synthetics from the regional mechanism for 8 P and 5 SH waveforms. The second line shows the fit of synthetics for the Harvard CMT mechanism. Strike, dip, rake, depth (km) and seismic moment (Nm) are shown above the P and SH focal mechanisms in each line.

two of the larger aftershocks of the Bhuj earthquake sequence (27 January and 28 January) had mechanisms (E-W trending thrusts) similar to that of the mainshock (Table 1). The 27 January (Mw 5.1) event occurred just north of the Kachcch Mainland fault, at the edge of the Banni Plain, and took up N-S compression along an E-W trending trust fault. The 28 January (Mw 5.7) event occurred on the north Wagad peninsula, probably on an E-W structure parallel to the northern boundary of the peninsula itself. Two of the aftershocks (8 February, 4 March) have well constrained strike slip mechanisms (Table 1) with N-S P-axes that can take up N-S shortening. The epicenters of these events to the north and south of the Wagad uplift, respectively (Figure 3), place them in the salt plains and tidal regions of the Rann. There is no obvious surface expression of the faults that ruptured in these small events (Mw 5.2 and 5.0 respectively). Wesnousky *et al.* (2001) reported that although they found no primary surface faulting reflecting large reverse motion, they did observe one tectonic rupture showing strike slip motion, along the western boundary of the Wagad uplift, near the town of Manfara. This surface rupture zone strikes NW for about 8 km, and shows primarily right lateral motion with up to 32 centimeters of slip. Given the location of the fault, between the Kachcch mainland and the Wagad uplift, Wesnousky *et al.* (2001) speculated that this strike slip rupture occurred on a pre-existing fault, related to a structural discontinuity or tear between the two uplifted blocks. The 3 February and 19 February aftershocks are both thrust events with a strike-slip component. The mechanism of the 3 February (Mw 5.1) event indicates either near-vertical slip on a high angle eastward dipping fault, or westward slip on a low angle southwest dipping fault. The mechanism of the 19 February (Mw 5.2) event is similar to that of the 3rd February, though the fault planes are reversed (the shallow plane dips east while the steep plane dips south west). The epicenters of these two events are both within the flat-lying tidal range of the Rann of Kachcch, and there is no obvious surface expression of the faults on which they occurred.

The source mechanism and depth can be further constrained by adding Pnl to the source mechanism inversion procedure. We have calibrated the Pnl propagation to the regional stations and are now incorporating Pnl in the source mechanism inversion routine.

REFERENCES

Antolik, M. and D.S. Dreger. (2001), Source rupture process of the 26 January, 2001 Bhuj, India, earthquake (M 7.6). *EOS Trans. AGU*, 82 (47), Fall Meet. Suppl.

Bapat, A., R.C. Kulkarni, and S.K. Gutha. (1983), Catalog of earthquakes in India and neighborhood from historical period up to 1979. Technical report, India. Soc. Earthq. Tech.

Bassin, B., G. Laske, and G. Masters, (2000), The current limits of resolution for surface wave tomography in North America. *EOS Trans. AGU*, 81: 897.

Bilham, R., (1998), Slip parameters for the Rann of Kachchh, India, 16 June 1819, earthquake, quantified from contemporary accounts. In I.S. Stewart and C. Vita-Finzi, editors, Coastal Tectonics, volume 146, pages 295-319. Geological Society, London, Special Publications.

Chung, W-Y. and H. Gao, (1995), Source parameters of the Anjar earthquake of July 21, 1956, India, and its seismotectonic implications for the Kutch rift basin. *Tectonophysics*, 242: 281-292.

Engdahl, E.R. and E.A. Bergman, (2001), Validation and generation of reference events by cluster analysis. In Proceedings of the 23rd Seismic Research Review: Worldwide Monitoring of Nuclear Explosions, Volume 1, pages 205-214. NNSA, DTRA.

Nolet, G., (1990), Partitioned waveform inversion ant two-dimensional structure under the Network of Autonomously Recording Seismographs. *J. Geophys. Res.,* 95: 8499-8512, 1990.

Reiter, D. T., M. Johnson, A. Rosca, C. Vincent (2001), Development of a regional 3-D velocity model of the Pakistan region for improved seismic event location. Final Report, Weston Geophysical, 27 p.

Sambridge, M. (1999), Geophysical inversion with a neighborhood algorithm - I: searching a parameter space. Geophys. J. Int., 138: 479-494.

Talwani, P. and A. Gangopadhyay, (2001), Tectonic framework of the Kachchh earthquake of 26 January 2001. *Seism. Res. Lett.,* 72: 336-345.

Wallace, T.C. (1986), Inversion of long period regional body waves for crustal structure. *Geophy. Res. Lett.*, 13.

Wesnousky, S. G., L. Seeber, T.K. Rockwell, V. Thakur, R. Briggs, S. Kumar, and D. Ragona (2001), Eight days in Bhuj: field report bearing on surface rupture and genesis of the 26 January 2001 earthquake in India. *Seism. Res. Lett.,* 72 514-523.

Yagi, Y. and M. Kikuchi (2001), Results of rupture process for January 26, 2001 western India earthquake (ms 7.9). WWW:http://wwweic.eri.u-tokyo.ac.jp/yuji/southindia/index.html, March 2001.